© Photos: DOI: 10.2516/ogst/2013139, IFPEN, X

Dossier

This paper is a part of the hereunder thematic dossier published in OGST Journal, Vol. 69, No. 1, pp. 3-188 and available online here

Cet article fait partie du dossier thématique ci-dessous publié dans la revue OGST, Vol. 69, n°1, pp. 3-188 et téléchargeable ici

DOSSIER Edited by/Sous la direction de : **C. Angelberger**

IFP Energies nouvelles International Conference / Les Rencontres Scientifiques d'IFP Energies nouvelles

LES4ICE 2012 - Large Eddy Simulation for Internal Combustion Engine Flows

LES4ICE 2012 - La simulation aux grandes échelles pour les écoulements dans les moteurs à combustion interne

Oil & Gas Science and Technology – Rev. IFP Energies nouvelles, Vol. 69 (2014), No. 1, pp. 3-188

Oil & Gas Science and Technology – Rev. IFP Energies nouvelles, Vol. 69 (2014), No. 1, pp. 107-128

DOI: 10.2516/ogst/2013142

IFP Energies nouvelles International Conference
Rencontres Scientifiques d'IFP Energies nouvelles

LES4ICE 2012 - Large Eddy Simulation for Internal Combustion Engine Flows
LES4ICE 2012 - La simulation aux grandes échelles pour les écoulements dans les moteurs à combustion interne

Investigation of Boundary Condition and Field Distribution Effects on the Cycle-to-Cycle Variability of a Turbocharged GDI Engine Using LES

S. Fontanesi[1]*, S. Paltrinieri[1], A. D'Adamo[1] and S. Duranti[2]

[1] *DIMeC - University of Modena and Reggio Emilia, Strada Vignolese 905, 41125 Modena - Italy*
[2] *CD-adapco Ltd., 200 Shepherds Bush Road, London, W6 7NL - England*
e-mail: stefano.fontanesi@unimore.it - stefano.paltrinieri@unimore.it - alessandro.dadamo@unimore.it - stefano.duranti@cd-adapco.com

* Corresponding author

Résumé — Études des effets des conditions aux limites et de la distribution des champs sur la variabilité cycle-à-cycle dans un moteur GDI turbocompressé en utilisant la LES — L'article présente les résultats préliminaires des activités numériques visant à caractériser la variabilité cycle-à-cycle d'un moteur DISI (Direct Injection Spark Ignition) turbochargé fortement downizé pour application automobile à haute performance en utilisant une version personnalisée du code commercial Star-CD sous licence de CD-adapco.

Au cours des études expérimentales au banc d'essai moteur, on a détecté une haute dispersion cycle-à-cycle, même pour des conditions de fonctionnement du moteur relativement stables à puissance maximale pleine charge, limitant ainsi les performances globales du moteur.

Malgré l'architecture complexe du moteur V-8, l'origine de la variabilité cyclique qui a été enregistrée ne pouvait pas être liée aux fluctuations cycliques de la dynamique du gaz entre les conduits d'admission et d'échappement. Plusieurs autres courbes de pression instantanées ont été mesurées à l'entrée du port d'admission et à la jonction de l'orifice d'échappement, montrant des différences presque négligeables en termes d'amplitude et de phase par rapport à celles dans le cylindre.

Pour explorer le potentiel de l'application de la technique LES pour l'analyse et la compréhension de la variabilité cycle-à-cycle, bien connue pour limiter fortement les performances globales du moteur, un travail numérique a été effectué et a concerné plusieurs cycles complets de simulations LES de cycles moteur consécutifs.

Malgré la précocité de l'étude, deux questions principales sont abordées dans l'article : l'analyse des causes possibles à l'origine de la variabilité cycle-à-cycle et l'influence des conditions aux limites sur la dispersion cyclique prévue.

En ce qui concerne la première question, une enquête détaillée a été conduite sur les champs instantanés locaux et globaux visant à identifier une possible hiérarchie des responsabilités d'un côté et les limites et les possibles améliorations de la procédure numérique adoptée de l'autre côté.

Quant au second point un ensemble de simulations réalisées, en appliquant des conditions expérimentales moyennées indépendantes du cycle, est comparé à celles résultant de l'application à l'admission et à l'échappement de pressions variables spécifiques au cycle, afin d'analyser l'influence des fluctuations des orifices sur l'historique des pressions dans le cylindre.

Les résultats sont aussi qualitativement comparés à ceux résultant d'un ensemble de simulations multi-cycle RANS utilisant la même dimension de grille afin de mieux mettre en évidence les potentialités exceptionnelles développées par la technique LES.

Abstract* — *Investigation of Boundary Condition and Field Distribution Effects on the Cycle-to-Cycle Variability of a Turbocharged GDI Engine Using LES — *The paper reports some preliminary results of a numerical activity aiming at characterizing cycle-to-cycle variability of a highly-downsized turbocharged DISI (Direct Injection Spark Ignition) engine for high-performance car applications, using a customized version of the commercial software Star-CD licensed by CD-adapco. During experimental investigations at the engine testbed, high cycle to cycle dispersion was detected even for relatively stable peak-power/full-load operations of the engine, thus limiting the overall engine performance.*

Despite the complex architecture of the V-8 engine, the origin of such cyclic variability could not be related to cyclic fluctuations of the gas-dynamics within the intake and exhaust pipes. Several subsequent acquisitions of the instantaneous pressure traces were measured at both the intake port entrance and exhaust port junction, showing almost negligible differences in terms of both amplitude and phasing compared to those within the cylinder.

In order to explore the potentials of the LES application to the analysis and understanding of the cycle-to-cycle variability, which notoriously strongly limits the overall engine performance, a numerical activity is carried out using full-cycle LES simulations over several subsequent engine cycles.

Despite the very early stage of the investigation, two main issues are addressed in the paper: the analysis of the possible causes originating the high cycle to cycle variability and the influence of the boundary conditions on the predicted cyclic dispersion.

Concerning the former aspect, a detailed investigation of local and global instantaneous fields is carried out aiming at identifying both a possible hierarchy of responsibilities on one side and limitations and possible improvements of the adopted numerical procedure on the other side.

Concerning the latter aspect, a set of simulations, performed applying cycle-independent averaged experimental conditions, is compared to those resulting from the application of cycle-specific variable pressure traces at both intake and exhaust sides, in order to analyze the influence of port fluctuations on the in-cylinder pressure history.

Results are also qualitatively compared to those resulting from a multi-cycle RANS simulation using the same grid-size, in order to better highlight the superior LES potentials.

NOMENCLATURE

BDC	Bottom Dead Center
BC	Boundary Condition
BFTDC	Before Firing Top Dead Center
CA	Crank Angle
CCV	Cycle-to-Cycle Variation
COVImep	Covariance of indicated mean effective pressure
DISI	Direct Injection Spark Ignition
EGR	Exhaust Gas Recirculation
ER	Equivalence Ratio
FBT	Flame Brush non-dimensional Thickness
FSD	Flame Surface Density
FTDC	Firing Top Dead Center
IMEP	Indicated Mean Effective Pressure
KLSA	Knock Limited Spark Advance
MFB	Mass Fraction Burnt
RMS	Root Mean Square
SA	Spark Advance
SEM	Synthetic Eddy Method
TE_sgs	Sub-grid scale Turbulent kinetic Energy
TDC	Top Dead Center
UHC	Unburnt hydrocarbons

INTRODUCTION

The analysis of consecutive in-cylinder pressure/time-histories inside an internal combustion engine clearly evidences the existence of non negligible variations from

one cycle to another. The phenomenon, usually referred to as "Cycle to Cycle Variation" (hereafter "CCV") must be carefully addressed in the design and control of spark-ignited engines in order to minimize its undesired effects on engine performance, emissions and durability.

On one hand, in fact, during relatively slow combustion cycles a risk exists of uncompleted combustion when the exhaust valve opens, or even misfire, which will result in dramatic increase of unburned hydrocarbon (UHC) emissions and lower efficiency. On the other hand, fast combustion cycles can undergo an increased risk of knocking, thus imposing an upper limit for performance-related parameters such as the boost pressure and/or the compression ratio for the chosen fuel. More generally, because of CCV, the spark advance properly matches only a few engine cycles, thus resulting in an undesirable loss of power and efficiency.

Several contributions available in literature [1, 2] show that the complete removal of CCV could lead up to a 10% increase in the power output of the engine for the same fuel consumption and tailpipe emission levels. Since the in-cylinder pressure rate is mainly related to combustion, pressure variations are primarily caused by alterations in the combustion process. Nevertheless, the combustion being affected by a complex sequence of preceding factors, the complete understanding of the actual origin of cyclic variability is usually far from being trivial.

This is particularly true for last generation multi-hole direct-injected engines, where instantaneous point-wise mixture stratification is strongly dependent on an unpredictable combination of:

– random broad-scale flow structures governing the transport of the fuel from the injector to the spark plug;
– cycle-dependent spray patterns varying in overall injected fuel mass, mass distribution among the nozzle holes, spray-plume penetration, etc.

Nevertheless, not only the mixture preparation affects the CCV of an engine. In fact, the early flame development is widely recognized to be extremely sensitive to mixture motion, exhaust gas concentrations at the spark plug gap at the time of ignition and at the spark plug region immediately after ignition, random flame kernel convection and heat transfer [3-8]. Since predicting and limiting cyclic variability is an issue of primary relevance for today's engine designers; CFD simulations can relevantly contribute, allowing the analysis of an extremely wide set of data, which are difficult to measure even in research laboratories. When facing CCV, traditional and well-established RANS techniques, resolving the phase- or ensemble-averaged Navier-Stokes equations, appear to be inadequate to capture the interactions among single instantaneous fields, which cannot be properly represented in terms of ensemble averaged quantities.

Large Eddy Simulation (LES) is widely recognized to be able to overcome the above mentioned RANS' limitations. In fact, LES preserves the intrinsic unsteady nature of the flow, where modeling is restricted to the application of a spatial filter to split resolved large scale structures from modeled small scale ones [9-15]. Nevertheless, LES applications to actual engine cases of practical interest are still limited, mainly because of the relevant computational costs [16-23]. In fact, despite the fact that most contributions deal with either simplified engine geometries [24-27] or idealized engine operations [28-31], very interesting and promising results are found in this paper, confirming the potentiality of the application of LES for the characterization of single cycle-resolved events typical of actual engine operations.

1 MODELING FRAMEWORK

1.1 Introduction

In the present paper, the authors investigate LES potentials through the characterization of CCV in a currently produced high performance engine, which is operated at full load and maximum power revolving speed.

In order to limit both the number of modeling uncertainties and the computational cost of the simulations, the so called "hybrid approach" of LES [13, 32, 33] is applied for what concerns the spray, where the interplay of the injected lagrangian parcels with the random LES flow fields can nevertheless result in "qualitative" CCV variations in the spray dynamics.

Furthermore, in order to exploit the applicability of LES to the research and development process, the grid size is limited by acting on the domain extent, the cell density and the cell spatial distribution. The resulting discretization appears to be consistent with indications from literature [22] and capable of resolving a reasonable set of flow scales, although grid-sensitivity analyses are planned in the near future. Attention is paid to the role played by the boundary conditions, through the comparison of two different modeling strategies. The former one relies on detailed cycle-dependent fast-response pressure measurements over 250 subsequent engine cycles at both the intake and exhaust ports, while the latter one is the more standardized practice of using cycle-independent traces derived from a 1D model of the whole engine.

Particularly, the first step of the analysis focuses on a comparison between LES and RANS simulations, in

order to discuss LES potentials in the analysis of CCV. The subsequent section focuses on the detailed analysis of 10 consecutive engine cycles, aiming both at characterizing the engine CCV and at trying to establish possible connections between CCV and in-cylinder pattern variations. In this section, merits and limitations of the adopted numerical approach are briefly discussed. In the last section of the paper, the attention is focused on boundary conditions choice for LES simulations.

1.2 LES Framework

As known, the full system of LES conservation equations for momentum, continuity, energy and species is filtered in space. Unclosed terms (sub-grid scale momentum, energy and species fluxes) appear in the equations and need to be modeled. The eddy viscosity Smagorisnky model [34] is adopted in this work with Smagorinsky constant $C_s = 0.14$. Wall modeling relies on standard wall functions.

1.3 Spray Modeling

Liquid fuel is injected in the form of individual droplets from separate injector holes. The injector holes and some relevant nozzle features are provided by the engine manufacturer and used within a Fortran routine to insert a population of previously atomized droplets of given diameter distribution and spatial velocity. The droplets interact with the gas phase by exchanging mass and energy [35-37].

Droplets' breakup is modeled by the Reitz Model [38] and droplet-wall interaction by the Bai model [39]. A detailed description of the tuning process of the spray models is far beyond the aim of the paper. Nevertheless, Figure 1, shows a comparison between computed and experimental sprays under quiescent conditions, highlighting the satisfactory agreement between numerical forecasts and measurements in terms of both spray shape and spray penetration.

1.4 Combustion Model

The mathematical model used here to describe the LES combustion is the ECFM-3Z [40, 41] adapted for LES studies [22, 42] and implemented in Star-CD solver V4.17 development. This choice is mainly justified by the model fundamental nature with a minimum amount of working assumptions, its known capabilities and the user's experience with ECFM-3Z accumulated in almost a decade, although the latter only within the RANS context.

In brief, the model belongs to the family of the coherent flame models where the flame surface density FSD (the flame surface area per unit volume) evolution is described by a balance equation which accounts for the effects of strain and curvature (both resolved and unresolved) along with the propagation of the flame itself in laminar unburnt gases zone.

$$\frac{\partial \Sigma}{\partial t} + \underbrace{\nabla \cdot (\tilde{u}\Sigma)}_{T_{res}} - \underbrace{\nabla \cdot \left[\sigma_c \left(D + \frac{\hat{\nu}_t}{Sc_t}\right) \nabla \Sigma\right]}_{T_{sgs}} + \underbrace{\nabla \cdot (S_d n \Sigma)}_{P}$$
$$= \underbrace{(\nabla \cdot \tilde{u} - n \cdot \nabla \tilde{u} \cdot n)\Sigma}_{S_{res}} + \underbrace{\Gamma\left(\frac{\hat{u'}}{S_l}, \frac{\hat{\Delta}}{\delta_l}\right) \frac{\hat{u'}}{\hat{\Delta}} \frac{\Sigma}{\sigma_c}}_{S_{sgs}} + \underbrace{S_d (\nabla \cdot n)\Sigma}_{C_{res}}$$
$$+ \underbrace{\beta S_l \frac{c^* - \bar{c}}{\bar{c}(1-\bar{c})} (\Sigma - \Sigma_{lam})\Sigma}_{C_{sgs}} \quad (1)$$

$T_{res}, T_{sgs}, P, S_{res}, S_{sgs}, C_{res}, C_{sgs}$ are the resolved transport, the sgs transport, the laminar propagation, the resolved strain, the sgs (sub-grid scale) strain, the resolved curvature and the sgs curvature, respectively. Gamma is an efficiency function that models the strain from sgs vortices onto the flame front and is taken from [43]:

$$\Gamma\left(\frac{\hat{\Delta}}{\delta_l}, \frac{\hat{u'}}{S_l}\right) = 0.75 \exp\left(-\frac{1.2}{\left(\hat{u'} S_l\right)^{0.3}}\right) \left(\frac{\hat{\Delta}}{\delta_l}\right)^{23} \quad (2)$$

with $\hat{\Delta}$, δl the combustion filter size and the laminar flame thickness, respectively.

In the LES version of the FSD equation (*Eq. 1*) the presence of resolved terms, that require sufficiently fine grid size to be represented, and the laminar propagation term are what distinguishes the above equation from the RANS counterpart: in fact, for this last, every term has to be modeled and the turbulence viscosity is assumed to be much higher than the molecular one. The resolved terms and the propagation term actually make it possible to simulate (as opposed to model) the evolution of the flame surface even for very low (sgs) turbulence levels which, for example, are not too infrequent situations in the early stages after spark ignition.

The FSD equation above is filtered at the combustion size rather than at the mesh size, where the combustion size is approximately equal to N_{res} times the grid size. With N_{res} typical = 5 and mesh characteristic sizes of approximately 0.5 mm, the combustion filter size is then approximately equal to the expected flame brush thickness. The use of this filter is justified by the circumstance

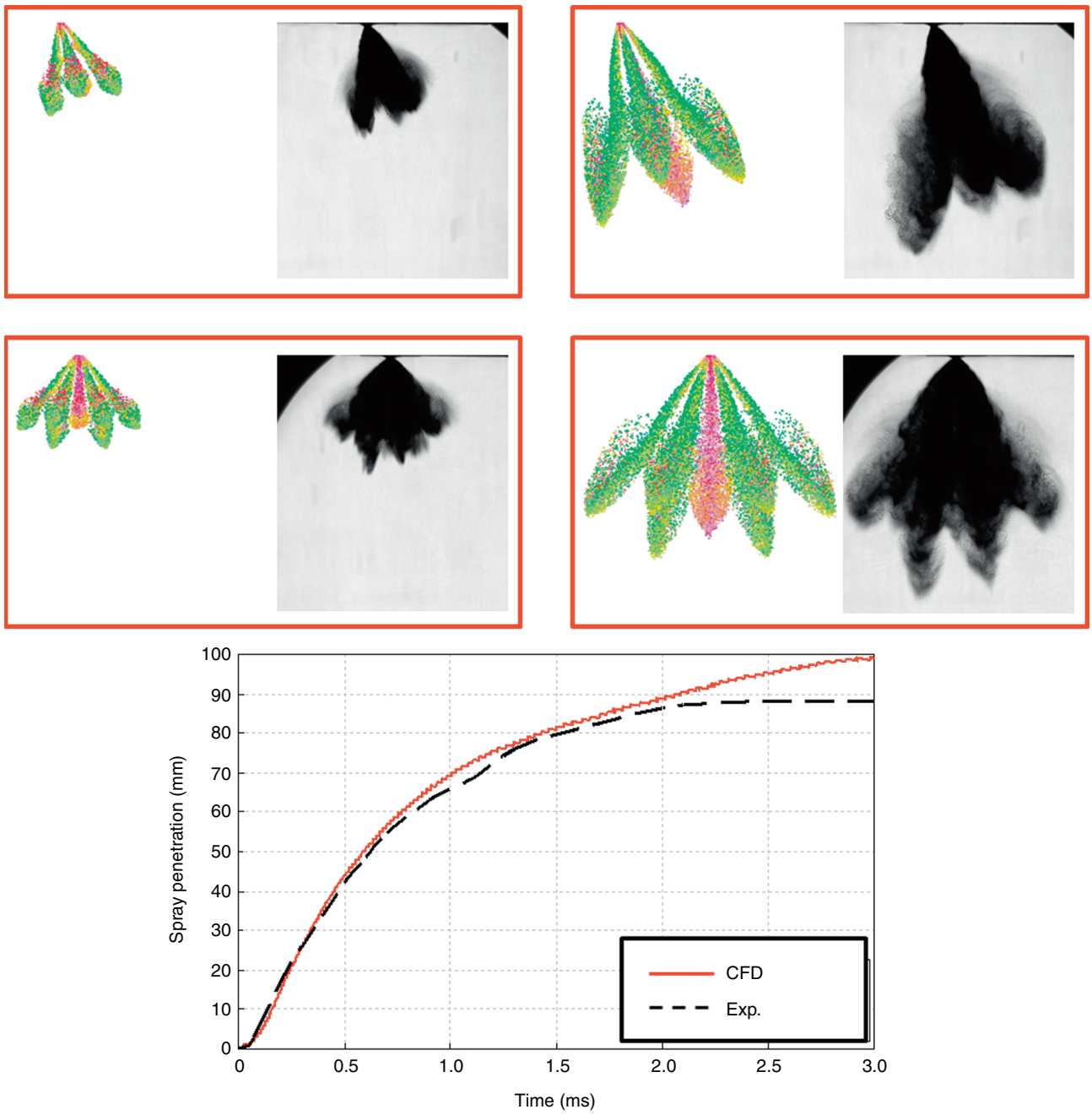

Figure 1

Lagrangian spray: CFD *versus* experiments. Spray shape (above), spray penetration (below).

that vortices smaller than the flame brush thickness are unable to wrinkle the flame [6] and, therefore, they limit the ability of the Gamma function to properly model the sgs strain rate.

Near solid surfaces, a simple wall quenching model is used in the Star-CD version, whereby production terms in the FSD equation are nullified when y+ is approximately 50.

As for ignition, the same model as in [22, 42] with minor modifications is adopted. Namely, a small profile of partially burnt gases is imposed at the time of the spark and around the spark location: the progress variable c is given an initial distribution as:

$$c(\boldsymbol{x},t) = \frac{c_0}{2}\left(1 - \tanh\frac{||\boldsymbol{x} - \boldsymbol{x}_{spk}||}{r_k}\right) \qquad (3)$$

with c_0 a tunable parameter and r_k the initial laminar flame kernel radius given by:

$$r_k = 15\delta_l \frac{T_b}{T_u} \tag{4}$$

The FSD from ignition is thus created:

$$\Sigma(\boldsymbol{x}, t) = S_m(t)\Xi \frac{c(1-c)}{\int c(1-c)dV} \tag{5}$$

then it is made to grow following a laminar theoretical growth law:

$$S_m(t) = 4\pi\left(r_k + \frac{T_b}{T_u} S_l\left(t - t_{ign}\right)\right)^2 \tag{6}$$

and wrinkled by turbulence with:

$$\Xi = 1 + \frac{1}{\sqrt{Re} - 1}\frac{\hat{u'}}{S_l}\left[\left(\frac{\hat{\Delta}}{\delta_l}\right)^{2/3} - 1\right] \tag{7}$$

the wrinkling factor, being derived from [43].

The local fuel consumption rate is thus computed as:

$$\dot{\omega}_f = \rho_u Y_f|_u S_l \Sigma \tag{8}$$

Numerically, all the terms in the FSD equation are implemented as sources except T_{res}, T_{sgs} and P, which are implemented as fluxes. This is important as the P term, for example, is actually an advection-like term with advection velocity equal to the laminar propagation speed; therefore it should be implemented as such for consistency and balancing reasons [44].

The user is also given a control on how "strong" the initial ignition profile must be, in the measure of how burnt (fully or partially) the gases in the ignition cell/s should be at the beginning. This is achieved by tuning the parameter c_0 in the initial c-profile Equation (3).

Ideally, as understood from [22, 42] one should minimize the impact of such user's imposed conditions on the numerical solution, and hence set the initial strength of the ignition as low as possible. However, in the present case-study it was found that too weak an ignition makes it impossible for a fully established front to form and for combustion to take place. The case is still under investigation, but it's likely that the main culprits are the very low levels of sgs turbulence near the spark plug, possibly caused by the plug obstruction (physical reason) or by the limitations of the Smagorinsky model, for which no velocity-strain means no turbulence (modeling reason). Imposing an initial fully burnt profile in a very limited portion of space substantially improved the results.

It is worth noting that such workaround has indeed modeling justifications: the FSD equation, which now is invoked and solved almost immediately after spark, is capable of handling 'laminar' fronts thanks to the propagation and the resolved strain and curvature terms [44]; its modeling capabilities are no inferior to, say, the ones of the flame wrinkling factor equation which is in [22, 42] applied during the ignition stages only.

Having said this though, further studies are underway to assess the effects of spark plug meshing, plug orientation, mesh local refinement, turbulence and LES ignition models on the ignition stage.

As for the heat transfer modeling, the "Angelberger" model for non-isothermal variable density flows is being used [45] whereby the wall heat flux is given by:

$$q_w = \frac{-\rho_w c_p u_\tau T_w}{T^+} \log\left(\frac{T}{T_w}\right) \tag{9}$$

with T^+ and T_w the non-dimensional temperature and the wall temperature, respectively. The presence of the log term in the above equation is the main difference with respect to the standard heat transfer model.

Wall temperatures are derived from a combination of:

- experimental data provided by the engine manufacturer;
- finite element calculations of the thermal field within the engine head and piston;
- 1D simulations of the whole engine for the intake and exhaust ports.

and then spatially averaged and uniformly applied to each domain surface.

1.5 Grid Construction

As stated above, the engine is a highly-downsized turbocharged DISI engine for high-performance car applications. In view of the complexity (both geometrical and fluid-dynamic), an effort is paid in order to find a trade-off between the computational costs and the result quality, in a tentative to apply LES to standard industry requirements and development times. As a consequence, the goal of mesh construction is twofold. The first one is to maintain a high quality in terms of grid size, resolution and homogeneity, whilst the second one is to perform the analysis in a reasonable computational time. Considering both these aims, the mesh, shown in Figure 2, meets the target of an average filter length of about 0.55 mm during the vast majority of the combustion process, allowing local filter values to have a deviation from it up to 100%.

The mesh is created using a trimming technique within the software es-ice, licensed by CD-adapco. The overall

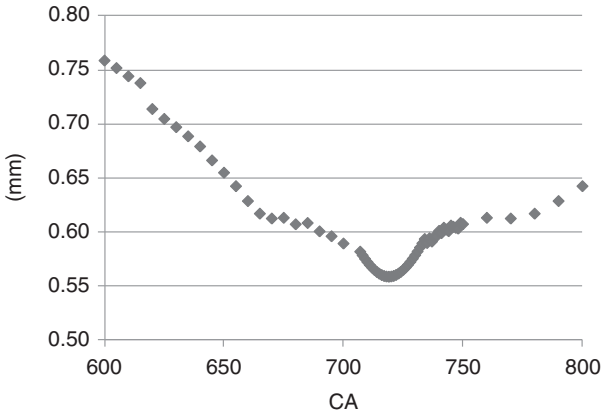

Figure 2
LES filter length.

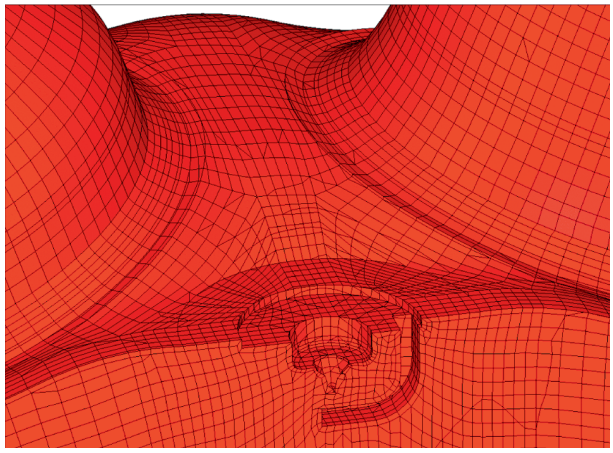

Figure 3
Computational grid at TDC, spark region.

result at BDC is a grid of more than 1.5 million cells of mainly hexahedral shape including the intake/exhaust ports. A zoomed view of the grid at the spark electrodes is depicted in Figure 3.

1.6 Initial Conditions

For all the subsequent analyses, initial conditions are obtained from a first RANS full-cycle simulation based on a combination of experimental data and 1-D engine model time-varying boundary conditions. This initial RANS cycle is tuned to closely match the average in-cylinder pressure trace resulting from 250 experimental pressure traces. The result is shown in Figure 4.

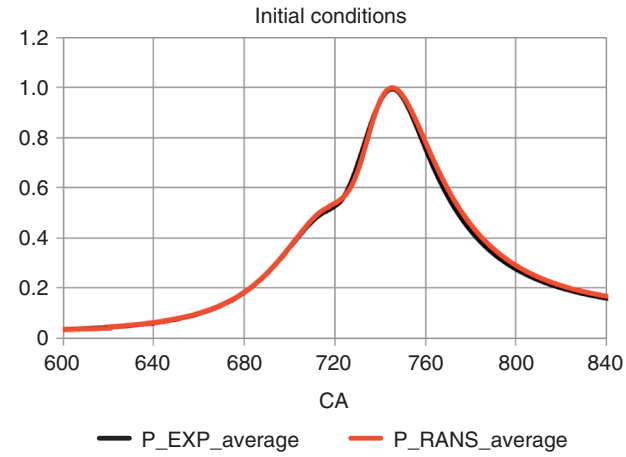

Figure 4
In-cylinder pressure, experimental *versus* 3D RANS.

2. RESULTS

2.1 LES/RANS Comparison

2.1.1 Introduction

As stated in the introduction, this first part of the activity is focused on the evaluation of LES and RANS potentials for the analysis of CCV. For this preliminary comparison, all the calculations are performed using cycle-specific pressure boundary conditions provided by the engine manufacturer and obtained by means of fast pressure transducers for "steady" engine operations over 250 subsequent engine cycles. As far as instantaneous temperature profiles are concerned, a periodic signal provided by a 1D model of the engine under investigation is used.

It might be argued that, as a result of variations in the imposed BC, even a RANS analysis would be able to capture CCV; to contradict this belief, parallel RANS and LES analyses are conducted with the same cycle-specific BC. The results from LES and RANS are analyzed in terms of in-cylinder CCV prediction capability.

2.1.2 Experimental Measurements

The cycle-specific boundary conditions, reported in Figure 5, are selected amongst the available 250 experimental cycles. Particularly, the range of consecutive cycles is chosen in order to cover a significant in-cylinder CCV, representative of the whole collection of data (*Fig. 6*).

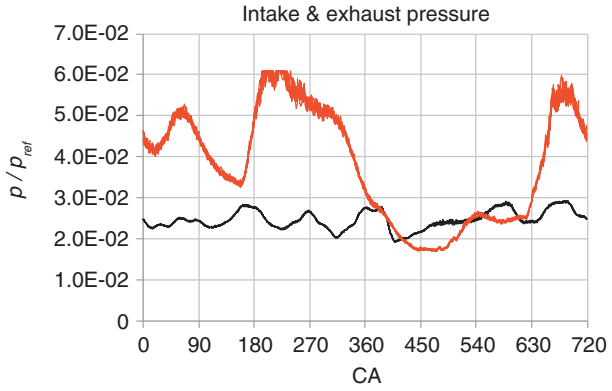

Figure 5

Cycle-specific pressure boundaries.

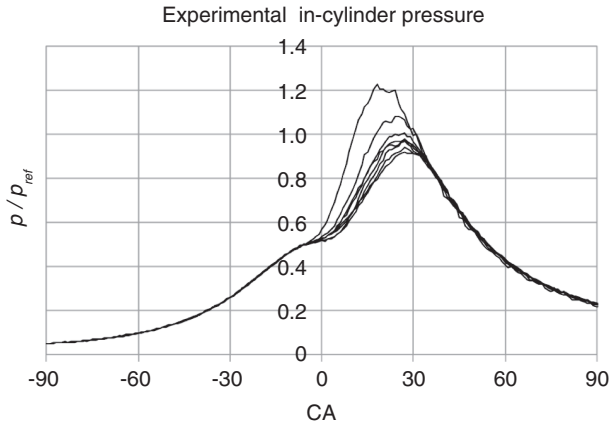

Figure 6

Selection of analyzed experimental cycles.

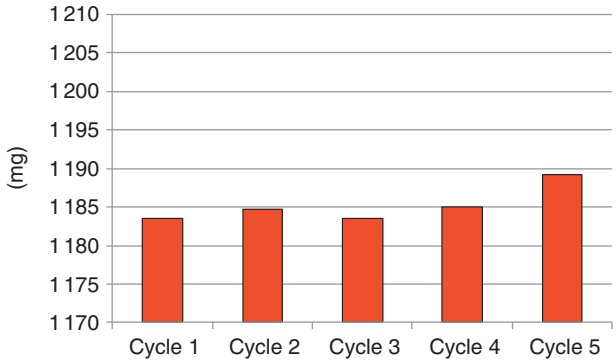

Figure 7

Trapped mass from RANS analyses.

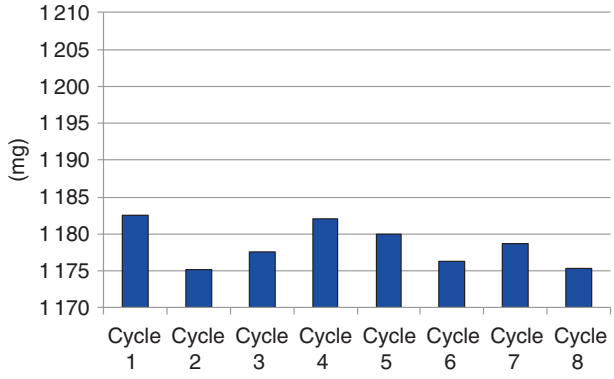

Figure 8

Trapped mass for LES analyses.

The variation in the intake and exhaust pressure traces is limited, and it will be discussed in the last part of this paper.

2.1.3 In-Cylinder Trapped Mass and Fuel Evaporation

A first macroscopic research for CCV causes focuses on the in-cylinder trapped charge. This parameter can be related to variations in the volumetric efficiency due to turbulent unsteadiness, random gas-dynamic effects, cylinder to cylinder variations.

Since, as stated earlier, the spray modeling is based on lagrangian RANS models, neither injected fuel mass nor droplet distribution are randomized for the CCV analysis; hence, the spray randomness is limited to the sole interaction with the cycle-specific flow structures, thus resulting in reduced variations. Furthermore, all the simulations are performed without adopting a liquid film model and the engine is operated with a very early start of injection, leading to a complete evaporation for every cycle analyzed. Small differences in the evaporated fuel are therefore primarily due to either the fuel convected back into the intake ports or the one that resides in the intake ports and is re-introduced at IVO by the gas dynamics.

Similar considerations can be extended to the heat transfer modeling.

The entrained mass of gas is evaluated at 20CAD BFTDC. The results show that small variations can be observed for both LES and RANS cycles in terms of trapped mass, thus enabling us to conclude that a very limited volumetric efficiency fluctuation is experienced even with cycle-varying boundary conditions (hereafter BC) (*Fig. 7, 8*).

TABLE 1
Trapped mass results, RANS *versus* LES

Mass trapped [mg]		
	Average	RMS
RANS	1 185.18	2.04
LES	1 178.44	2.90

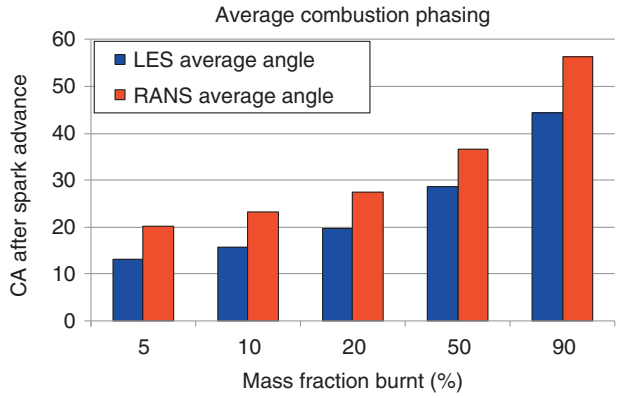

Figure 9
Average crank angle for given MFB for RANS and LES.

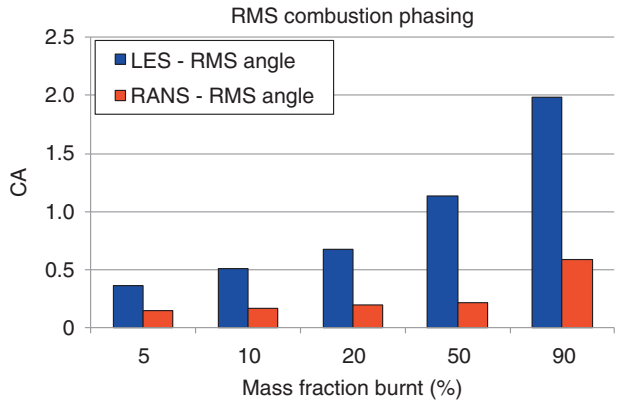

Figure 10
Root mean square for given MFB for RANS and LES.

As visible from the above pictures, the population of investigated cases is different for the two approaches. In fact, since RANS shows an almost null variation in terms of in-cylinder pressure trace, only 5 consecutive cycles are modeled and the attention is shifted towards the more promising LES cases.

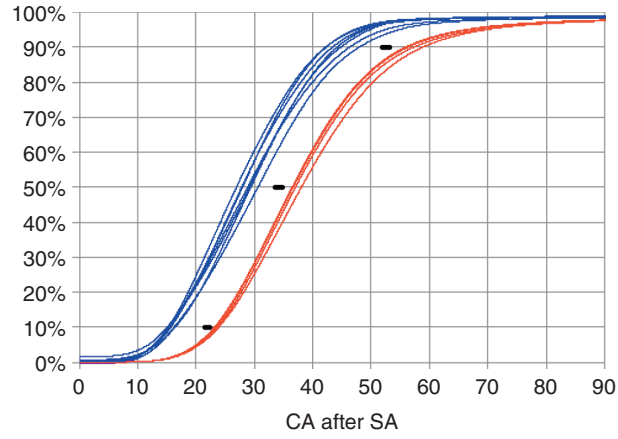

Figure 11
Mass fraction burnt for RANS and LES & experimental range.

The average and RMS characterization of the trapped mass shows a reduced breathing capability for the LES simulations, due to the highest backpressure in the exhaust, decreasing the scavenging effectiveness. This is an expected consequence of a major difference between RANS and LES ignition models, which was briefly explained in the modeling section and will be further commented later. The different ignition treatment leads to a non-negligible phase shift between RANS and LES and to subsequent overall higher in-cylinder pressures for the LES analyses.

As expected, the RMS comparison shows a higher variation for the LES cases, even if its amplitude is somehow comparable to that predicted by RANS.

2.1.4 Combustion Phasing Comparison

The combustion phasing is at first analyzed through Mass Fraction of fuel Burnt (hereafter MFB) as a function of crank angle. This analysis is a first phenomenological estimation of the different combustion developments due to variations in the spark relative air to fuel ratio, turbulence, flow field etc. MFB evolution is tracked at 5%, 10%, 20%, 50% and 90% of the overall burnt mass.

As expected, RANS results show a relevant reduction in the RMS of the fuel consumption compared to LES ones, although very modest differences can be observed as a consequence of cycle-varying BCs. However, the fluctuations of the resulting combustion process are much more limited than those resulting from a dedicated

LES modeling (flow field and combustion model, together with cycle-varying BCs).

It is now once again important to underline the major difference in the ignition models used for RANS and LES. As stated earlier, the ignition phase is modeled as instantaneous and is therefore relatively stiff (the current LES framework is still under development). Flame variations, due to the interaction with the LES flow field, are taken into account through the FSD equation, where additional randomness brought in by the breakdown and arc phase are, at the present stage, neglected. On the contrary, the RANS combustion model is provided with a very simple and consolidated algebraic ignition model, yet capable to model the CA lapse between the spark discharge and the flame kernel growth. As this model is based on local physical variables (density, unburnt temperature etc.), it should intrinsically be able to introduce a moderate degree of variation in the combustion development according to the cycle-varying BCs.

The ensemble average of MFB is strongly influenced by the mentioned difference between the LES/RANS ignition models, showing an advance in the combustion development for the LES cycles of about 7-8 CAs with respect to the average RANS one. A better match between LES and experiments could be achieved through a slight phase-shift of the imposed spark release angle; the authors believe that such a tuning process is far beyond the aim of the present study. A specific activity on the ignition model is being developed in order to reduce, or even eliminate, the presented discrepancy [46].

Despite the above considerations for ignition, it is indeed remarkable to observe a higher level of RMS for the LES cases, which tends to approach the experimentally detected values especially for the mid and the late portions of the combustion process, as reported in Table 2. On the contrary, no significant CCV can be observed in the 0%-10% of MFB for RANS cycles.

2.1.5 In-Cylinder CCV

The experimental in-cylinder pressure traces for the analyzed cycles are shown in Section 2.1.2, Figure 5. The RANS and LES results for the same cycles are reported in Figures 12 and 13 respectively.

TABLE 2
RMS value for significant combustion phasing

	10% MFB	50% MFB	90% MFB
Experimental	1.90	2.47	2.38
RANS	0.16	0.21	0.58
LES	0.61	1.43	1.98

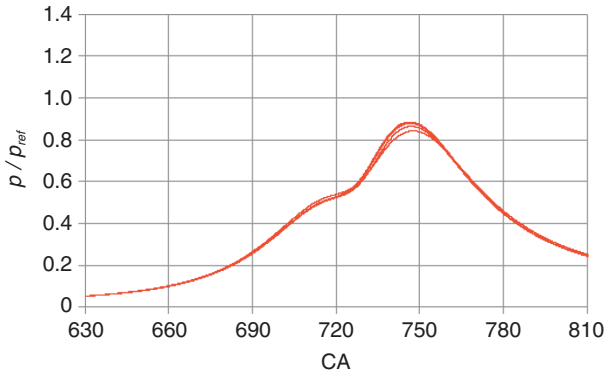

Figure 12
RANS in-cylinder pressure results.

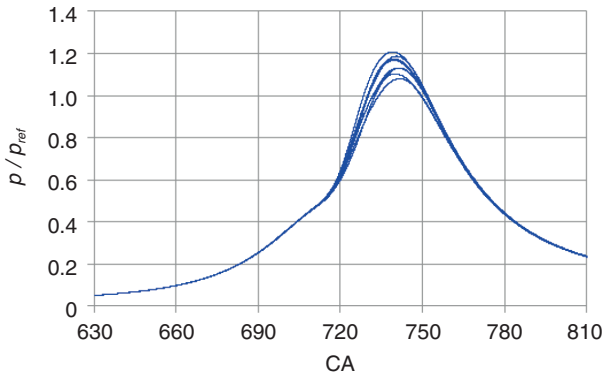

Figure 13
LES in-cylinder results.

As previously anticipated, the focus of this analysis is not intended to match either the exact value of peak pressure or the combustion phasing as well. For these specific results a better agreement with experiments could easily be obtained by means of a better tuning of both RANS and LES ignition models. The reason why this tuning is not of interest at the present stage is that the analysis is focused on the comparison between RANS and LES in terms of CCV prediction. Despite the above discussed moderate stiffness in the LES ignition treatment, the laminar phase of flame development is correctly solved by the FSD equation.

Ignition effects are strong on the combustion phasing, as it can be observed comparing RANS and LES, but it is not supposed to significantly influence the CCV of combustion which is the main focus of the present work. It is in fact evident that the RMS of peak pressure for

TABLE 3
In-cylinder pressure analysis for experimental, RANS and LES analysis

	Experimental		RANS analysis		LES analysis	
	Average	RMS (% of average)	Average	RMS (% of average)	Average	RMS (% of average)
Normalized pressure Peak	0.98	5.06	0.87	1.89	1.15	3.79
CA (P_{max}) ATDC	26.63	2.79	26.75	1.82	20.41	4.82
Normalized IMEP	0.22	2.32	0.23	0.43	0.25	1.49

LES is very similar to the experimentally measured one. On the contrary, the RANS value is much smaller, thus enforcing the idea of the inadequacy of a RANS approach to capture CCV, even with cycle-varying BCs. Similar considerations can be stated focusing on the crank angle at which the maximum pressure is observed. Its amplitude of variation (again expressed by its RMS) is much closer to the experimental CCV for LES, while the RANS analyses result in very poor variations.

As far as IMEP is concerned, which is usually considered as an overall indicator resembling all the fluid-dynamic processes of the engine (both scavenging and combustion), the average value is strongly affected by the shift resulting from the ignition model. This explains the higher value for LES. Concerning RMS, the faster combustion development, which is always promoted for LES cases, dampens cyclic variability because of the relatively shorter time of exposition to the fluctuations of the flow field. Nevertheless, despite this intrinsic smoothing in terms of CCV, the LES value is promising and is much higher than the analogous results for RANS.

The stability of the operating point is well confirmed by the cycle mapping on the Matekunas diagram [23, 47], reported in Figure 14, *i.e.* a characteristic way to express the stability of the operating point. Matekunas identified a zone of linear correlation between p_{max} and CA (p_{max}) where a stable and fast combustion is detected.

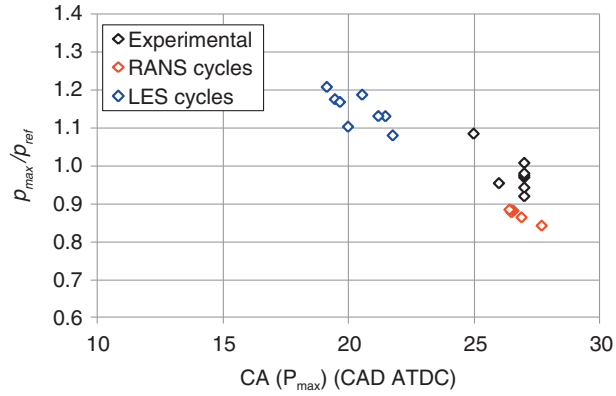

Figure 14
Matekunas diagram for the analyzed cycles.

2.1.6 Conclusions

Experimental and cycle-varying pressure boundary conditions are used for both a standard RANS multi-cycle analysis and a LES one.

The results in terms of variance of in-cylinder pressure peak (both amplitude and phasing) show a promising agreement between LES simulations and experimental data, thus confirming LES potential in investigating the inherent unsteadiness of the in-cylinder phenomena. This is particularly significant considering that a crucial phase of the combustion process, *i.e.* the flame kernel formation, is still under modeling development and it is not yet completely influenced by local physical values in LES analyses.

RANS cycles show a very limited amount of CCV, despite the application of cycle-varying BC, and this confirms the impossibility to capture the intrinsic unsteadiness of the in-cylinder phenomena.

2.2 LES Analysis of CCV

2.2.1 Introduction

The second step of the analysis underlines LES potential in investigating the origin of highly transient phenomena such as CCV and Cylinder-to-Cylinder Variation.

In particular, LES is used as a tool for sensitivity analysis to variations in engine variables. As stated earlier, all the results are obtained through the sole effect of turbulent dispersion among the cycles. In fact, since cycle-specific experimental pressure traces at the intake and exhaust ports have been provided by the engine manufacturer only in recent times, boundary conditions are kept fixed along 10 consecutive LES cycles. Furthermore, in view of the lack of *ad-hoc* investigations and detailed experimental measurements, also the spray features, spark time and spark position are kept fixed for all the modeled cycles. As a consequence, the forecasts cannot be 100% representative of either the experimental pressure traces and their variance, since all the listed previously parameters contribute themselves to produce in-cylinder CCV. Despite the above limitation, a wide set of variables is taken into account in order to determine which are possibly the main causes of CCV in DISI engines, both at the spark time occurrence and throughout the whole combustion process.

2.2.2 Correlation Coefficient Analysis

To gain a first insight into CCV, a correlation analysis is used to shed light on possible connections between some relevant operating parameters. A correlation coefficient between a field variable X and a set of either global or local variables Y_j (where the suffix j can in turn be representative of *EGR*, equivalence ratio, sgs turbulent energy *TE*, magnitude of the flow field velocity, etc.) is therefore introduced, its proximity to 1 expressing a high correlation between two analyzed factors. Its formulation is the following:

$$p_i(X, Y_j) = abs\left(\frac{\mathrm{cov}(X, Y_j)}{\sqrt{\mathrm{var}(X) \cdot \mathrm{var}(Y_j)}}\right) \qquad (10)$$

Through this analysis, the parameters mostly influencing CCV can emerge. Results are shown in Figures 15 and 16, where the peak cylinder pressure is correlated to average in-cylinder and spark located fields respectively (see *Tab. A1* in Appendix A for a list of abbreviations).

The observation of Figures 15 and 16 highlights some interesting issues:

– none of the globally averaged parameters seems to exhibit a dominant connection with the in-cylinder pressure peak. In fact, all the correlation coefficients are well below 0.5;
– among the global parameters, temperature, EGR concentration and sgs turbulent energy seem to play a slightly major role;

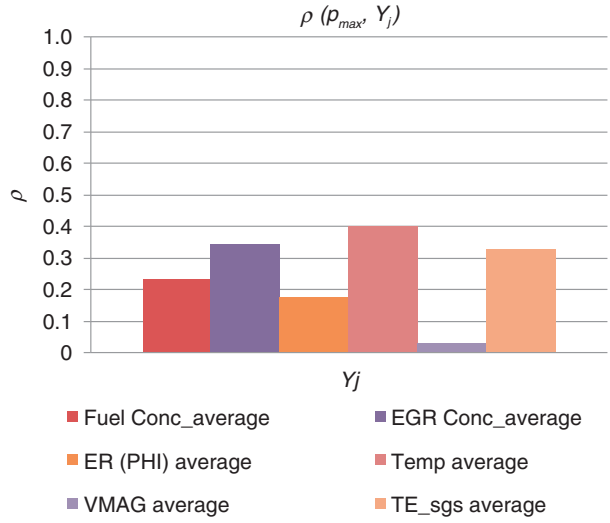

Figure 15

Correlation analysis, p_{max} *versus* average in-cylinder fields.

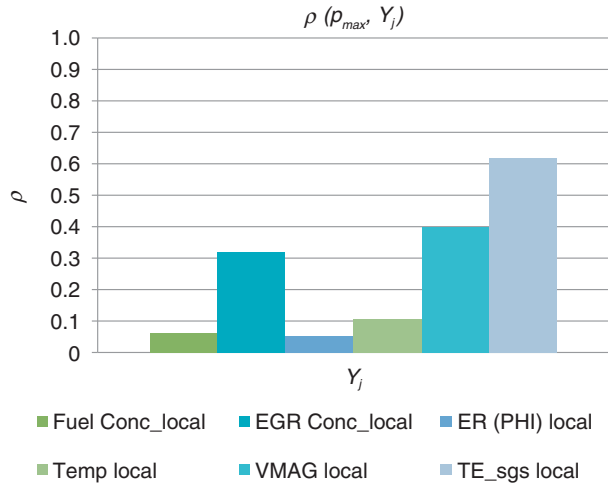

Figure 16

Correlation analysis, p_{max} *versus* spark-plug fields.

– similar considerations can be drawn for local spark-plug centered fields, as visible in Figure 16. Among the whole set of parameters, local velocity magnitude and sgs turbulent energy are the only parameters above 0.4.

Despite the correlation analysis is at a very early stage and a wider population of cycles is needed to assess its effectiveness, it seems to be a promising tool to summarize the huge amount of information deriving from the CFD analyses and create high-order and low-order hierarchies among the many investigated parameters.

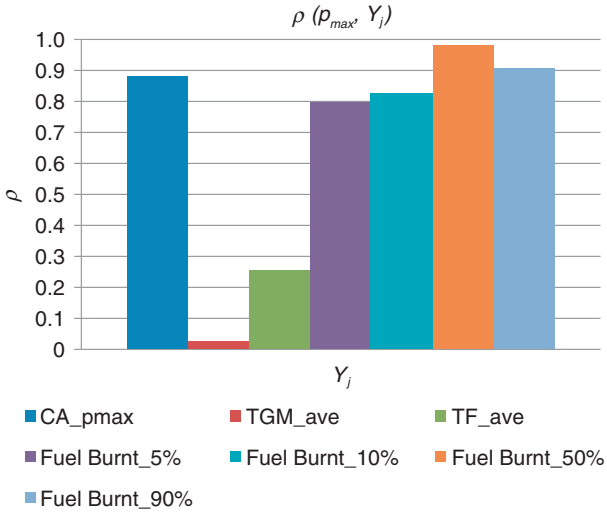

Figure 17

Correlation analysis, p_{max} *versus* MFB.

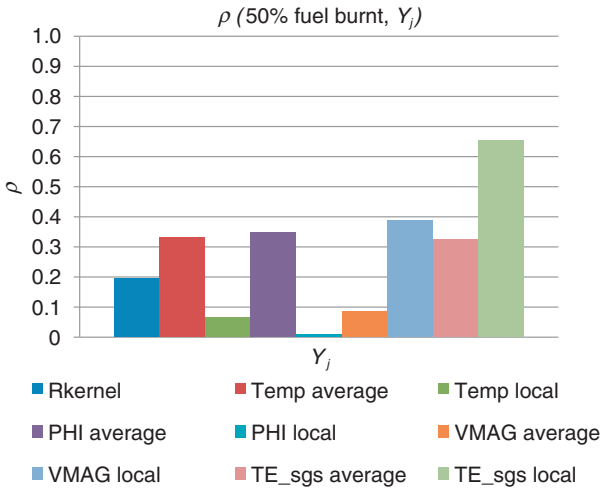

Figure 18

Correlation analysis, 50% MFB *versus* global and spark-plug fields.

As an example, Figures 17 and 18 confirm the well known high degree of correlation between peak pressure and the crank angle location of the 50% MFB, which in turn proves to be well correlated to both global and local sgs turbulent energy.

2.2.3 Analysis of Possible CCV Causes

Figure 19 confirms once again LES capability of both capturing CCV and matching the experiments in terms

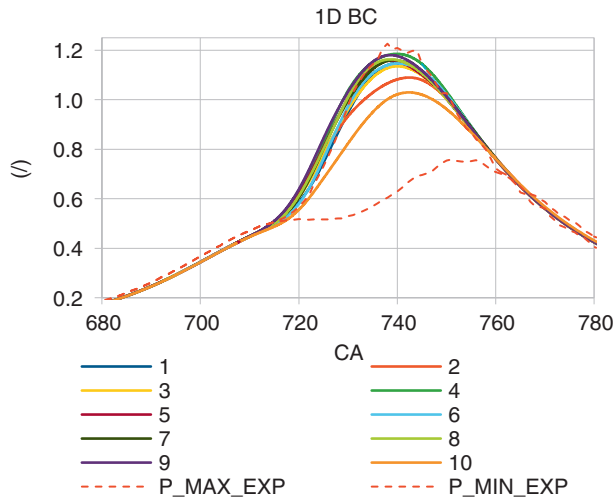

Figure 19

Average in-cylinder pressure, LES simulation and experimental extremes.

of peak pressure amplitude and phasing. All of the pressure traces fall within the experimental range marked by dashed red lines. A small advance is visible for the early stages of combustion, this difference being a consequence of the ignition model modification and explaining why most of the pressure signals fall into the upper portion of the experimental range.

Nevertheless, CCV is relevant and the pressure peak varies of about 20%. At the present stage, the CCV shown is the minimum achievable CCV in an actual engine. In fact, this value is produced only by turbulent randomness and it does not take into account others factors which could increase the CCV itself.

Despite some clear indications on the possible origin of CCV come out from the previously reported correlation coefficient analysis, in the present section additional ones are introduced by evaluating averaged fields progressively experienced by the flame front while advancing within the combustion chamber. Particularly, in the following paragraphs attention is paid to:

- trapped fuel mass,
- local equivalence ratio at the flame front,
- tumble,
- local velocity field at the flame front,
- local turbulent energy at the flame front,
- flame surface extension.

Trapped fuel mass does not change relevantly among the cycles, as shown in Table 4. Therefore, it cannot be considered a major cause of CCV. A further confirmation comes from the observation of the 10th cycle, in

which the in-cylinder pressure trace is the lowest one although the trapped fuel is not the minimum.

On the contrary, ER distribution deserves special attention. Figure 20 shows the variation among the 10 cycles on a plane section corresponding to the geometrical symmetry plane.

All the pictures refer to the spark time crank angle. Particularly, among all cycles, the 3rd and the 6th are characterized by slightly lean and very rich mixtures respectively. The ER distribution seems to be related to the intensity of the tumble motion (computed as the angular speed of the direct tumble vortex) within the combustion chamber at the end of the compression stroke, which is depicted in Figure 21.

TABLE 4
LES trapped fuel mass

Cycles	Trapped gas mass (kg)
1	0.001150
2	0.001154
3	0.001153
4	0.001152
5	0.001149
6	0.001151
7	0.001150
8	0.001151
9	0.001153
10	0.001150

A correlation between the intensity of the motion and the ability to properly mix the injected fuel with the surrounding air seems to be detected, since it is when tumble is the weakest that the charge shows its lowest homogeneity. A correlation seems therefore to be established between charge motion and ER distribution, as visible from the comparison between Figures 21 and 22, where the Average ER distribution seen by the flame while it is expanding towards the wall.

It is well documented in literature that such a result should relevantly influence the combustion development. Thus, a significant difference in terms of in-cylinder pressure trace should be expected especially at the early stages of the flame development. Nevertheless, the observation of the CFD in-cylinder pressure around FTDC reported in Figure 19 seems to indicate that either the modification to the ignition model partially smoothes the ER effects or ER does not relevantly influence the early stages of the combustion, as highlighted in the previous section, where the correlation coefficient between equivalence ratio at the spark and in-cylinder pressure evolution was found to be very low. The first explanation appears to be the most favourable, since further development (still in progress and therefore not reported in the present paper) [46] indicates that both spark grid and initial kernel size are key factors to govern the sensitivity to pointwise distributions. For the present study, and considering the adopted mesh resolution, the reduced sensitivity dims the pressure peak and peak phase shift between the 3rd and 6th cycle, as visible in Figure 19. Another interesting observation can be made on the interaction between the flow field and the

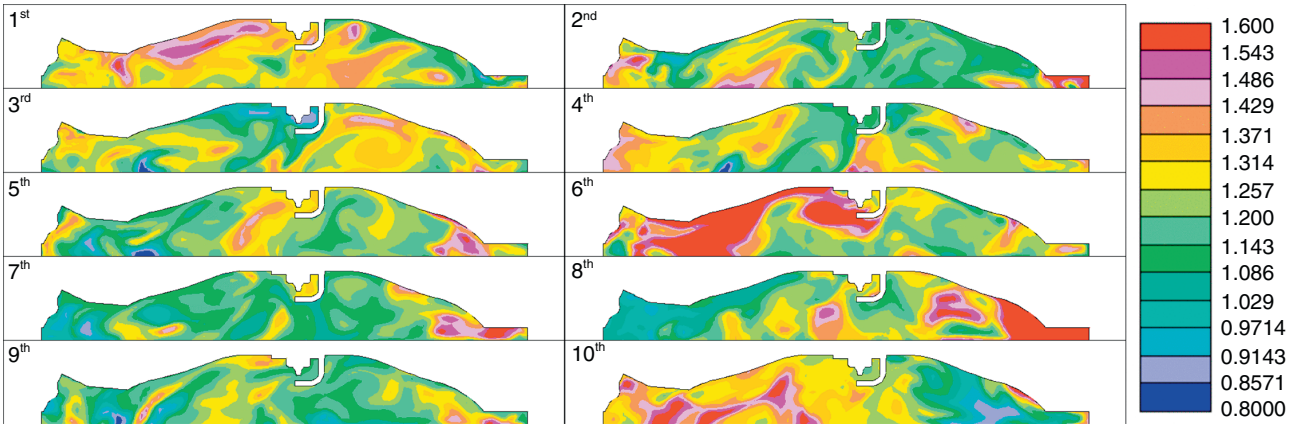

Figure 20
LES ER distribution, symmetry plane vertical section.

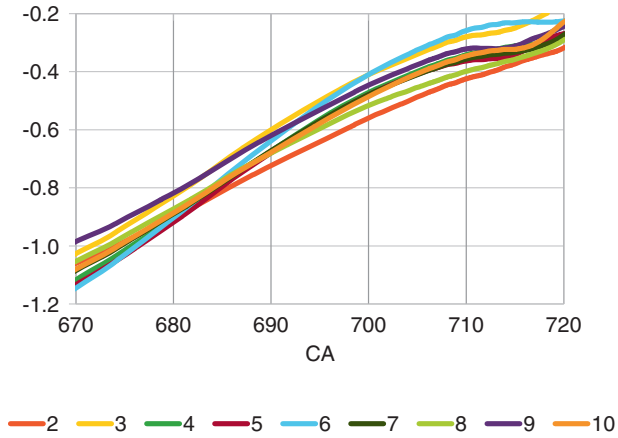

Figure 21

LES tumble variation. Direct tumble – during combustion.

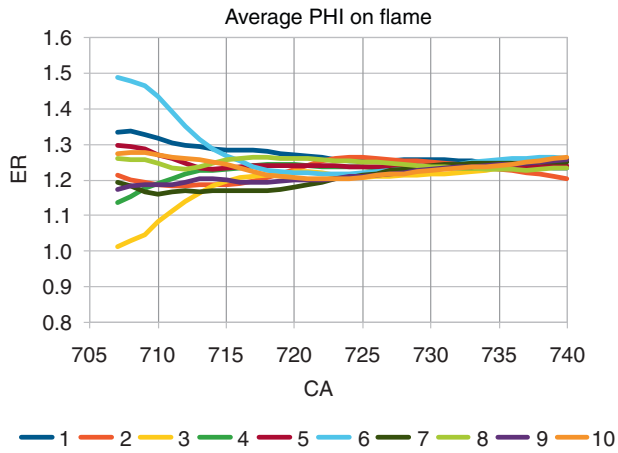

Figure 22

LES average ER distribution.

flame kernel just after the spark time. In fact, the sequence of images in Figure 23, where the in-cylinder velocity field is superimposed to the flame front iso-surface again on a plane section corresponding to the symmetry plane, shows that for a few crank angles after the spark the flame kernel is transported by the flow field and it is either stretched or compressed by it.

Particularly, Figure 23 shows the comparison between the lowest and the highest computed cycles (in terms of pressure peak), clearly highlighting the role played by the flame kernel convection away from the electrodes on the capability of the flame front to spread throughout the combustion chamber and to consume the available fuel. The strong interaction between the local flow fields (both large scale and sgs) is confirmed by the qualitative analyses of the sequences of pictures reported in Appendix B at the end of the paper. In the pictures, images are reported for the non-dimensional Flame Brush Thickness *FBT* defined as:

$$FBT = c \cdot (1 - c) \tag{11}$$

where c is the progress variable. FBT distributions on a plane section perpendicular to the cylinder axis (see Appendix C) for two different crank angles (10° after spark ignition and 30° after spark ignition) are compared for the ten LES cycles, confirming the high sensitivity of the LES model to variations in the field patterns and its capability in capturing CCV.

Similar considerations cannot be clearly evidenced if velocity magnitude averaged over the flame surface is used, as shown in Figure 24.

While it is difficult to establish clear connections between the in-cylinder pressure trace and the velocity field over the flame surface, a much more evident effect seems to be played by the average turbulent energy, again computed over the flame front surface and visible in Figure 25, confirming the indications from the correlation coefficient analysis. Sgs turbulent energy is a straightforward indication of both the chance for the flame to be fed by fresh fuel and the increase of its thickness. A trade-off between wrinkling and feeding effects is needed in order to have the best compromise in terms of flame speed, thus pressure development.

In conclusion, results show that the in-cylinder velocity field strongly interacts with the flame development, mainly for two reasons:

– the direction towards which the flame front is transported has a strong impact on its propagation;
– velocity field is directly linked to resolved turbulent energy thus to flame wrinkling.

As a further confirmation of the second statement, the "fastest" cycle in terms of combustion development is compared to the "slowest", showing a substantial difference in terms of flame surface extension between the two cycles, as reported in Figure 26.

2.3 Influence of Boundary Conditions

2.3.1 Comparison Between Cycle-Averaged and Cycle-Specific BC

The aim of the last step of the analysis is to quantify the correlation between CCV of the pressure signal at the boundaries and in-cylinder CCV (in terms of peak pressure, combustion phasing, etc.).

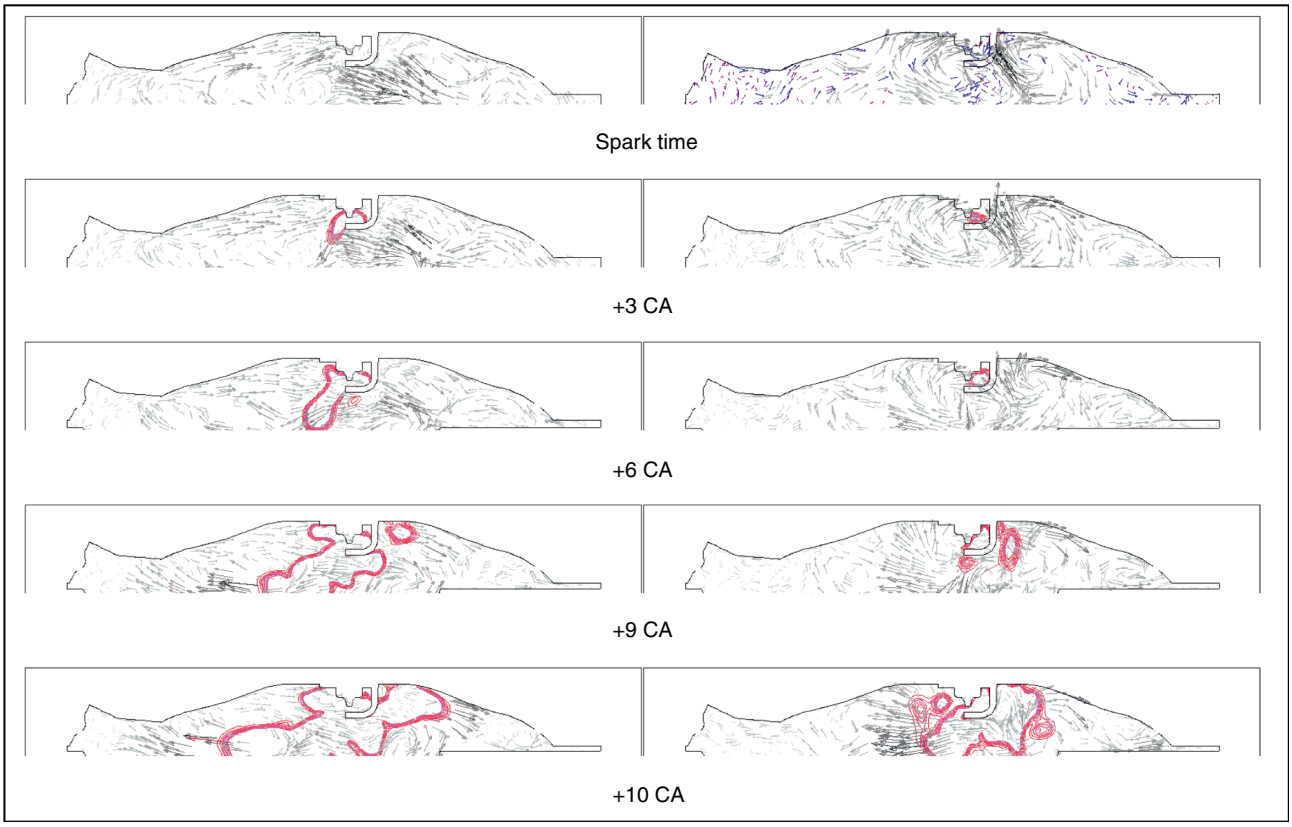

Figure 23

Flame front and velocity vectors from spark timing. 4th cycle is the one showing the highest pressure peak (left hand side), 10th cycle is the one showing the lowest pressure peak (right hand side).

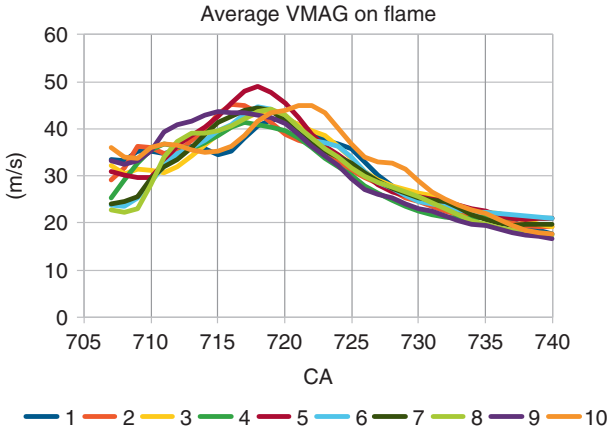

Figure 24

LES average velocity magnitude on flame.

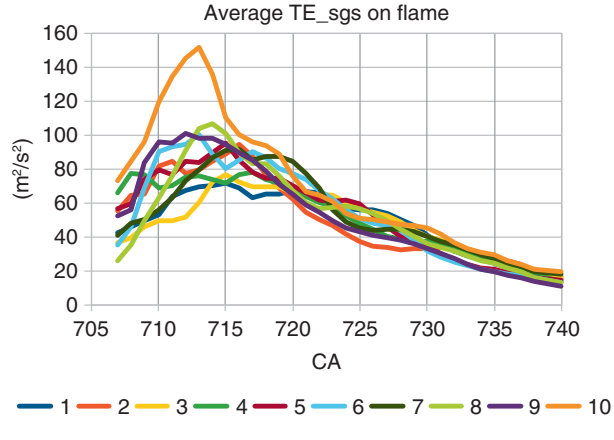

Figure 25

LES average sgs Turbulent Energy (TE).

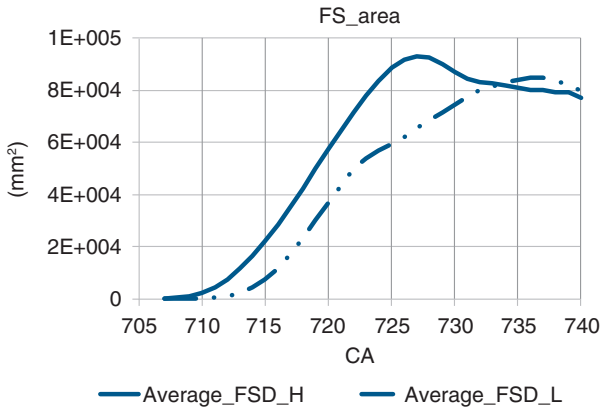

Figure 26

Flame surface, highest cycle *versus* lowest one.

TABLE 5

Boundary condition effects comparison

	LES BC_EXP	LES BC_1D
Trapped mass gas (mg)	1 178.44	1 151.21
RMS mass gas trapped (mg)	2.90	1.72
Mass burnt 5% (CA after SA)	13.04	12.98
RMS 5% (CA)	0.36	0.83
Mass burnt 10% (CA after SA)	15.73	15.66
RMS 10% (CA)	0.61	0.91
Mass burnt 50% (CA after SA)	28.59	27.94
RMS 50% (CA)	1.43	1.46
Mass burnt 90% (CA after SA)	44.40	43.35
RMS 90% (CA)	1.98	1.78
Peak pressure (p/p_{ref})	1.15	1.14
RMS pressure (%)	3.79	4.12
CA (p_{max}) (CA after SA)	34.41	33.95
RMS CA (p_{max}) (CA)	0.98	1.44
Normalized IMEP	0.25	0.25
RMS IMEP (%)	1.49	1.16

If intake and exhaust signal cyclic variability plays a relevant role on the randomization of in-cylinder patterns, two alternatives appear for the LES analysis of CCV. The former is the use of experimentally driven cycle-dependent information, the latter relies on the application of synthetic or random boundary flow structures aiming at artificially reproducing the signal randomness.

On the contrary, in case of limited correlation between in-cylinder CCV and pressure boundary fluctuations (mainly based on the hypothesis of a dominating random turbulence generation at the valve curtain region), the use of periodic pressure and temperature profiles (such as those typically derived from 1D simulations of the whole engine) at both the intake and exhaust side of the domain, as reported in the previous section, is possible. While waiting for the consolidation of recent promising approaches [48], two different simulation sets are therefore carried out in order to evaluate the boundary effects on CCV. The former is based on the application of experimentally derived cycle-dependent pressure profiles, while the latter is based on cycle-repeatable 1D information, relying just on the intrinsic capability of LES to capture turbulence randomness. It is worthwhile to remark that, for both numerical approaches, a constant level of turbulence intensity is imposed at the boundaries, and none of the methods for reproducing synthetic or random boundary flow structures is adopted in this work. This choice is made by the authors for the sake of generality and assuming a negligible influence of the local flow structures imposed at the boundaries on the in-cylinder turbulence. The influence of the adopted boundary conditions is assessed through a set of variables characterizing both the combustion process and the global engine behaviour in terms of average values and RMS. Table 5 reports the comparison between the two procedures: on the leftmost column, the variables and their RMSs are listed, on the central column ("LES BC_VAR") results are reported for the cycle-specific experimentally derived pressure traces, while the rightmost column ("LES BC_CONST") refers to the 1-D simulation derived cycle-independent boundary conditions. Despite small differences exist between experimental and 1D boundary conditions, the gap is limited within a few percentage points. Whereas said, the best way to construe results is to compare the standard deviation of a generic variable: results exhibit that no substantial differences are imputable to fluctuations at the boundaries. A significant example of this can be found in terms of CA location for prescribed MFB

where, for the same combustion phasing, no clear trends can be relieved between the two BC approaches in terms of standard deviation.

At this point, fluctuation on BC did not bring to a wider CCV so the use of time-varying BC deriving from 1D simulations appears to be a reasonable choice to qualitatively investigate in-cylinder CCV, while strongly simplifying the problem set up.

CONCLUSION

The paper highlights LES potential in characterizing cycle-to-cycle variability in internal combustion engines. In particular, the study focuses on a highly-downsized turbocharged DISI engine for high-performance car application operated at full load, peak power engine speed, which exhibited high cycle to cycle dispersion at the engine testbed. A detailed numerical activity is carried out using full-cycle LES simulations over several subsequent engine cycles to investigate the possible origins of such cycle-to-cycle variability. This non-trivial task is carried out through the use of correlation coefficients and local patterns experienced by the flame front, aiming at establishing a hierarchy of responsibilities among the many local and global instantaneous fields. All the analyses are carried out using Star-CD licensed by CD-adapco. Each of the 20 LES full-cycle simulations (10 using experimentally derived boundary conditions and 10 using 1D simulation information) are performed on 60 cores of a linux cluster available at the University of Modena and Reggio Emilia, with computational times slightly less than one week for each of the full 720 CA.

Additional cycles are in progress in order to increase the statistical population for the analyses.

The influence of the choice of boundary conditions on the predicted cyclic dispersion is also discussed through the comparison between a cycle-independent pressure trace derived from a 1D model of the engine and cycle-specific experimental information provided by the engine manufacturer. No significant differences emerge between the two approaches, confirming the intrinsic capability of LES to capture turbulence randomness.

Some modeling issues on ignition, which might be caused by low levels of sgs turbulence near the spark plug due to the plug obstruction or by limitations of the adopted Smagorinsky model are briefly commented in the paper and will be the object of future investigations. Despite the early stage of the activity, the analyses confirm LES ability in correctly capturing mutual interdependencies between instantaneous flow patterns.

At the present stage of development, this modeling framework and the inherent level of CCV shows promising potential in modeling random phenomena such as knock and misfire. Particularly, knock is currently being investigated in a parallel activity based on coupled LES and chemical kinetics simulations. Detailed results of this activity can be found in [49].

REFERENCES

1 Young M. (1981) Cyclic Dispersion in the Homogeneous-Charge Spark-Ignition Engine—A Literature Survey, SAE Technical Paper 810020, doi: 10.4271/810020.

2 Ozdor N., Dulger M., Sher E. (1994) Cyclic Variability in Spark Ignition Engines A Literature Survey, SAE Technical Paper 940987, doi: 10.4271/940987.

3 Hamai K., Kawajiri H., Ishizuka T., Nakai M. (1988) Combustion fluctuation mechanism involving cycle-to-cycle spark ignition variation due to gas flow motion in S. I. Engines, *Int*, *Symp. Combust.* **21**, 1, 505-512.

4 Hill P.G., Kapil A. (1989) The relationship between cyclic variations in spark-ignition engines and the small structure of turbulence, *Combust. Flame* **78**, 2, 237-247.

5 Aleiferis P.G., Hardalupas Y., Taylor A.M.K.P., Ishii K., Urata Y. (2004) Flame chemiluminescence studies of cyclic combustion variations and air-to-fuel ratio of the reacting mixture in a lean-burn stratified-charge spark-ignition engine, *Combust. Flame* **136**, 1-2, 72-90.

6 Bates S. (1989) Flame Imaging Studies of Cycle-by-Cycle Combustion Variation in a SI Four-Stroke Engine, SAE Technical Paper 892086, doi: 10.4271/892086.

7 Nwagwe I.K., Weller H.G., Tabor G.R., Gosman A.D., Lawes M., Sheppard C.G.W., Wooley R. (2000) Measurements and large eddy simulations of turbulent premixed flame kernel growth, *Proc. Combust. Inst.* **28**, 1, 59-65.

8 Barlow R.S. (2007) Laser diagnostics and their interplay with computations to understand turbulent combustion, *Proc. Combust. Inst.* **31**, 1, 49-75.

9 Rogallo R., Moin P. (1984) Numerical Simulation of Turbulent Flows, *Annu. Rev. Fluid Mech.* **16**, 99-137.

10 Meneveau C., Katz J. (2000) Scale-invariance and turbulence models for large-eddy simulation, *Annu. Rev. Fluid Mech.* **32**, 1-32.

11 Pope S.B. (2004) Ten questions concerning the large-eddy simulation of turbulent flows, *New J. Phys.* **6**, 35.

12 Lesieur M., Métais O., Compte P. (2005) *Large-Eddy Simulations of Turbulence*, Cambridge University Press, UK.

13 Rutland C.J. (2011) Large-eddy simulations for internal combustion engines – a review, *Int. J. Engine Res.* **12**, 421-451.

14 Pitsch H., Desjardins O., Balarac G., Ihme M. (2008) Large-eddy simulation of turbulent reacting flows, *Prog. Aerosp. Sci.* **44**, 6, 466-478

15 Knudsen E.W., Pitsch H. (2010) Large-Eddy Simulation for Combustion Systems: Modeling Approaches For Partially Premixed Flows, *TOTHERJ* **4**, 76-85.

16 Goryntsev D., Sadiki A., Klein M., Janicka J. (2009) Large eddy simulation based analysis of the effects of cycle-to-cycle variations on air–fuel mixing in realistic DISI IC-engines, *Proc. Combust. Inst.* **32**, 2, 2759-2766.

17 Haworth D.C. (1999) Large-Eddy Simulation of in-Cylinder Flows, *Oil Gas Sci, Technol. - Rev. IFP* **54**, 2, 175-185.

18 Haworth D.C., Jansen K. (2000) Large-eddy simulation on unstructured deforming meshes: towards reciprocating IC engines, *Comput. Fluids* **29**, 5, 493-524.

19 Fogleman M., Haworth D.C., Rempfer D., Lumley J.L. (2004) Application of the Proper Orthogonal Decomposition to Datasets of Internal Combustion Engine Flows, *J. Turbul.* **5**, 1-18.

20 Dugué V., Gauchet N., Veynante D. (2006) Applicability of Large Eddy Simulation to the Fluid Mechanics in a Real Engine Configuration by Means of an Industrial Code, SAE Technical Paper 2006-01-1194, doi: 10.4271/2006-01-1194.

21 Adomeit P., Lang O., Pischinger S., Aymanns R., Graf M., Stapf G. (2007) Analysis of Cyclic Fluctuations of Charge Motion and Mixture Formation in a DISI Engine in Stratified Operation, SAE Technical Paper 2007-01-1412, doi: 10.4271/2007-01-1412.

22 Vermorel O., Richard S., Colin O., Angelberger C., Benkenida A., Veynante D. (2009) Towards the understanding of cyclic variability in a spark ignited engine using multi-cycle LES, *Combust. Flame* **156**, 8, 1525-1541.

23 Granet V., Vermorel O., Lacour C., Enaux B., Dugué V., Poinsot T. Large-Eddy Simulation and experimental study of cycle-to-cycle variations of stable and unstable operating points in a spark ignition engine, *Combust. Flame* **159**, 4, 1562-1575.

24 Celik I., Yavuz I., Smirnov A., Smith J., Amin E., Gel A. (2000) Prediction of in-cylinder turbulence for IC engines, *Combust. Sci. Technol.* **153**, 1, 339-368.

25 Devesa A., Moreau J., Poinsot T., Helie J. (2004) Large Eddy Simulations of Jet/Tumble Interaction in a GDI Model Engine Flow, SAE Technical Paper 2004-01-1997, doi: 10.4271/2004-01-1997.

26 Keskinen J., Vuorinen V., Kaario O., Larmi M. (2012) Large Eddy Simulation of the Intake Flow in a Realistic Single Cylinder Configuration, SAE Technical Paper 2012-01-0137, doi: 10.4271/2012-01-0137.

27 Liu K., Haworth D.C. (2010) Large-eddy simulation for an axisymmetric piston-cylinder assembly with and without swirl, *Flow Turbul. Combust.* **85**, 279-307.

28 Goryntsev D., Sadiki A., Klein M., Janicka J. (2008) Large eddy simulation based analysis of the effects of cycle-to-cycle variations on air–fuel mixing in realistic DISI IC-engines, *Proc. Combust. Inst.* **32**, 2, 2759-2766.

29 Enaux B., Granet V., Vermorel O., Lacour C., Thobois L., Dugue V., Poinsot T. (2010) Large Eddy Simulation of a motored single-cylinder piston engine: numerical strategies and validation, *Flow Turbul. Combust.* **86**, 2, 153-177.

30 Rezaei R., Pischinger S., Adomeit P., Ewald J. (2012) Numerical investigation of the effect of swirl flow in-homogeneity and stability on Diesel engine combustion and emissions, *Int. J. Engine Res.* **13**, 5, 482-496.

31 Vitek O., Macek J., Tatschl R., Pavlovic Z., Priesching P. (2012) LES Simulation of Direct Injection SI-Engine In-Cylinder Flow, SAE Technical Paper 2012-01-0138, doi: 10.4271/2012-01-0138.

32 Hu B., Jhavar R., Singh S., Reitz R.D., Rutland C.J. (2007) Combustion modeling of Diesel combustion with partially premixed condition, SAE Technical Paper 2007-01-0163, doi: 10.4271/2007-01-0163.

33 Arai J., Oshima N., Oshima M., Ito H., Kubota M. (2007) Large Eddy Simulation of Spray Injection to Turbulent Flows from a Slit Nozzle, *J. Fluid Sci. Technol.* **2**, 3, 601-610.

34 Smagorinsky J. (1963) General circulation experiments with the primitive equations, *Mon. Wea. Rev.* **91**, 99-164.

35 Bird R.B., Stewart E.W., Lightfoot E.N. (1960) *Transport Phenomena*, John Wiley & Sons, New York.

36 El Wakil M.M., Ueyhara O.A., Myers P.S. (1954) A theoretical investigation of the heating-up period of injected fuel droplets vaporizing in air, NACA Technical Note 3179.

37 Ranz W.E., Marshall W.R. (1952) Evaporation from drops – Parts I and II, *Chem. Eng. Prog.* **48**, 3, 141-146; 173-180.

38 Reitz R., Diwakar R. (1986) Effect of Drop Breakup on Fuel Sprays, SAE Technical Paper 860469, *SAE Trans.* **95**, 3, 218-227.

39 Bai C., Gosman A.D. (1995) Development of Methodology for Spray Impingement Simulation, SAE Technical Paper 950283, doi: 10.4271/950283.

40 Colin O., Benkenida A. (2004) The 3-Zone Extended Coherent Flame Model (ECFM3Z) for computing premixed/diffusion combustion, *Oil Gas Sci. Technol. – Rev. IFP* **59**, 6, 593-609.

41 Duclos J.M., Bruneaux G., Baritaud A. (1996) 3D modelling of combustion and pollutants in a 4-valve SI engine; effect of fuel and residuals distribution and spark location, SAE Technical Paper 961964, doi: 10.4271/961964.

42 Richard S., Colin O., Vermorel O., Benkenida A., Angelberger C., Veynante D. (2007) Towards large eddy simulaiton of combustion in spark ignition engines *Proc. Combust. Inst.* **31**, 3059-3066.

43 Colin O., Ducros F., Veynante D., Poinsot T. (2000) A thickened flame model for large eddy simulations of turbulent premixed combustion, *Phys. Fluids* **12**, 7, 1843-1863.

44 Dugué V. (2007) Étude du potentiel des simulations aux grandes échelles pour la prédiction des variations cycliques dans les moteurs automobiles, *Doctorate Thesis*, École centrale de Paris, Châtenay-Malabry, France.

45 Angelberger C., Poinsot T., Delhay B. (1997) Improving Near-Wall Combustion and Wall Heat Transfer Modeling in SI Engine Computations, SAE Paper 972881, doi: 10.4271/972881.

46 Fontanesi S., Paltrinieri S., Tiberi A., D'Adamo A. (2013) LES multi-cycle analysis of a high performance GDI engine, SAE Technical Paper 2013-01-1080, doi: 10.4271/2013-01-1080.

47 Matekunas F.A. (1983) Modes and Measures of Cyclic Combustion Variability, SAE Technical Paper 830337, doi: 10.4271/830337.

48 Pera C., Richard S., Angelberger C. (2012) Exploitation of Multi-Cycle Engine LES to Introduce Physical Perturbations in 1D Engine Models for Reproducing CCV, SAE Technical Paper 2012-01-0127, doi: 10.4271/2012-01-0127.

49 Fontanesi S., Paltrinieri S., D'Adamo A., Cantore G., Rutland C. (2013) Knock Tendency Prediction in a High Performance Engine Using LES and Tabulated Chemistry, SAE Technical Paper 2013-01-1082.

Manuscript accepted in December 2012
Published online in November 2013

APPENDIX A

TABLE A1
List of acronyms and abbreviations for the correlation coefficient analysis

Name	Meaning
CA_pmax	Crank angle at which the maximum peak of pressure occurs
TGM_ave	Trapped gas mass
TF_ave	Trapped fuel
Fuel Burnt_5%	Crank angle at which the 5% of burnt gas occurs
Fuel Burnt_50%	Crank angle at which the 50% of burnt gas occurs
Fuel Burnt_90%	Crank angle at which the 90% of burnt gas occurs
Fuel Conc_Average	Average fuel concentration value when valves are already closed
Fuel Conc_Local	Local fuel concentration value close to the spark plug
EGR Conc_Average	Average EGR concentration value when valves are already closed
EGR Conc_Local	Local EGR concentration value close to the spark plug
ER (PHI) Conc_Average	Average Equivalence Ratio (PHI) concentration value when valves are already closed
E.R. (PHI) Conc_Local	Local Equivalence Ratio (PHI) concentration value close to the spark plug
Temp average	Average temperature inside the chamber at the spark time occurrence
Temp local	Local temperature inside the chamber at the spark time occurrence close to the spark plug location
VMAG average	Average velocity magnitude inside the chamber at the spark time occurrence
VMAG local	Local velocity magnitude inside the chamber at the spark time occurrence close to the spark plug location
TE_sgs average	Average turbulent kinetic energy inside the chamber at the spark time occurrence
TE_sgs local	Local turbulent kinetic energy inside the chamber at the spark time occurrence close to the spark plug location
Rkernel	Kernel radius calculated by the ignition model

APPENDIX B

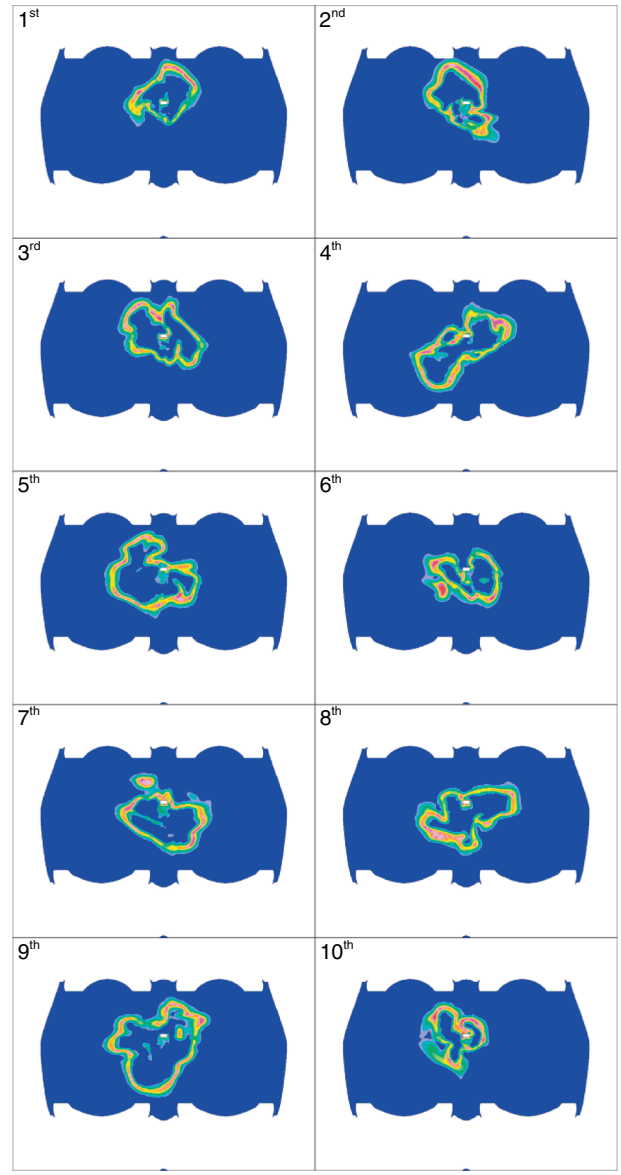

Figure A1
$c * (1 - c)$, 10 CA after SA.

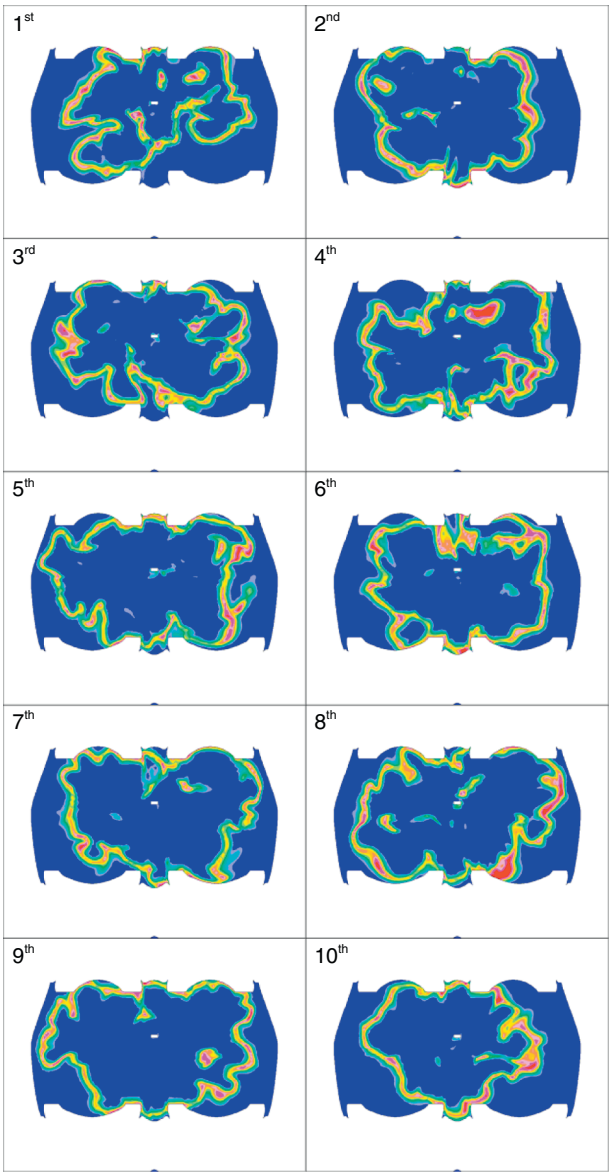

Figure A2
c * (1 – c), 20 CA after SA.

APPENDIX C

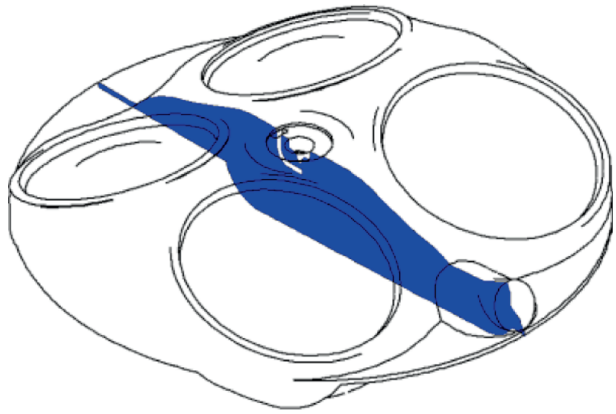

Figure A3
Vertical plane section.

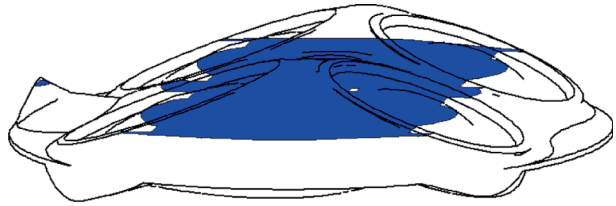

Figure A4
Horizontal plane section.